

Response to comments

Paper #: *essd-2022-180*

Title: *GWL_FCS30: global 30 m wetland map with fine classification system using multi-sourced and time-series remote sensing imagery in 2020*

Journal: *Earth System Science Data*

Reviewer #2

The submitted manuscript provides a global wetland map including inland and tidal sub-classes based on remote sensing data. Currently, we are still lacking a multi-class global wetland data including inland and tidal wetlands simultaneously, and the map produced by this work provides valuable information for related wetland studies. The manuscript is well-written and easy to follow. Above all, I recommend their publication provided that a moderate revision is carried out.

[Great thanks for the positive comments. The manuscript has been further improved based on your and other two reviewers' comments and suggestions.](#)

1. Wetlands are classified as inland or coastal wetlands in this study, and the latter includes mangroves, salt marshes, and tidal flats. For these three wetland types, the term “tidal wetlands” is more appropriate than “coastal wetlands”, for example, in Murray et al., 2022. Coastal wetlands include other terrestrial and shoreline constituents like riparian wetlands and tidal freshwater marshes, but not just mangroves, salt marshes and tidal flats. As such, I suggest using “tidal wetlands” to make the classification system more accurate.

[Great thanks for your useful suggestion. The ‘coastal wetland’ has been changed as the ‘tidal wetland’ in our fine wetland classification system as:](#)

Table 2. The description of wetland classification system in this study

Category I	Category II	Description
Tidal wetland	Mangrove	The forest or shrubs which grow in the coastal blackish or saline water
	Salt marsh	Herbaceous vegetation (grasses, herbs and low shrubs) in the upper coastal intertidal zone
	Tidal flat	The tidal flooded zones between the coastal high and low tide levels including mudflats and sandflats.
Inland wetland	Swamp	The forest or shrubs which grow in the inland freshwater
	Marsh	Herbaceous vegetation (grasses, herbs and low shrubs) grows in the freshwater
	Flooded flat	The non-vegetated flooded areas along the rivers and lakes
	Saline	Characterized by saline soils and halophytic (salt tolerant) plant species along saline lakes
	Permanent water	Lakes, rivers and streams that are always flooded

2. Section 2.4: This section is about generating validation samples, thus should be moved to the “Accuracy assessment” section as a validation step. Another thing is how did the authors determine the size of total validation samples (i.e., 18,701)?

Great thanks for the comment. First, Based on the suggestion, the section 2.4 of how to generate the global validation samples has been moved to the Section 4.3 Accuracy Assessment.

Then, as for how to determine the size of total validation samples, we combined the stratified random sampling method and the proportions of various land-cover types to determine the sample size of each land-cover type based on the work of Foody et al. (2009) and Olofsson et al. (2014) as:

$$n = \frac{(\sum W_h \sqrt{p_h(1-p_h)})^2}{V + \sum W_h P_h(1-P_h)/N}$$

where N is the number of pixel units in the study region; V is the standard error of the estimated overall accuracy that we would like to achieve, $V = (d/t)^2$ ($t = 1.96$ for a 95% confidence interval, $t = 2.33$ for a 97.5% confidence interval, and d is the desired half-width of the confidence interval); W_h is the weight distribution of class h ; p_h is the producer's accuracy. These sample size calculations should be repeated for a variety of choices of V and p_h before reaching a final decision. We try to achieve producer's accuracies of 0.9 of non-wetland class and 0.8 of the seven wetland classes. Meanwhile, using the parameters of $d = 0.0125$, $t = 2.33$, the sample size can be determined as approximately 18500. In addition, there is a little uncertainty for interpreting the validation points, so we randomly generate 20000 validation points over the globe and then discard 1299 uncertain points (these disagreement points over five experts), so a total of 18701 validation points are used to assess the GWL_FCS30-2020 performance.

Pontus Olofsson, G. M. F. (2014). Good practices for estimating area and assessing accuracy of land change. *Remote Sensing of Environment*, 148(25), 42-57, <https://doi.org/10.1016/j.rse.2014.02.015>.

Foody, Giles M. "Sample size determination for image classification accuracy assessment and comparison." *International Journal of Remote Sensing* 30.20 (2009): 5273-5291.

This amount seems disproportionately less than the number of training samples (more than 20 million).

As for the unbalance of the training samples and validation samples, it is mainly because our training and validation samples are completely independent. Specifically, **we combined many pre-existing global wetland datasets to automatically derive the training samples over the globe while the validation points must be interpreted by visual interpretation.** As we all known, collecting validation points through visual interpretation is time-consuming and labor-intensive, therefore, we cannot to interpret a large amount of validation points.

(3) Lines 250-255: The tidal flat samples were collected from the global tidal flat map (Murray et al., 2019), and thus would suffer from the inherent error of the data. Several studies found that Murray's tidal flat map failed to distinguish between nearshore ponds and tidal flats, mainly because these ponds also have water-level variations (Jia et al., 2021; Zhang et al., 2022). The error of commission (i.e., classifying ponds into tidal flats) is also indicated in the tidal flat map generated by this study, as shown in the upper panels of Fig. 13. I suggest the authors mask out ponds and lakes from their tidal flat map because it would substantially improve the accuracy. There is a new dataset that provides global lakes and reservoirs may be helpful: Khandelwal et al. 2022.

Great thanks for the comment and useful suggestion. Yes, we agree that the Murray's tidal flat suffered the commission error especially over the nearshore ponds. Based on your suggestion, the new global lakes and reservoirs dataset is used to further optimize tidal flat layer in our GWL_FCS30.

In addition, as the tidal flats were demonstrated to overestimate some coastal ponds as the tidal flats, the global lake and reservoir dataset, developed by Khandelwal et al. (2022), was applied to optimize the tidal flat.

The local comparisons in the Figure 16 shows that the updated GWL_FCS30 dataset has better performance than Murray's tidal flat products in excluding these ponds and lakes.

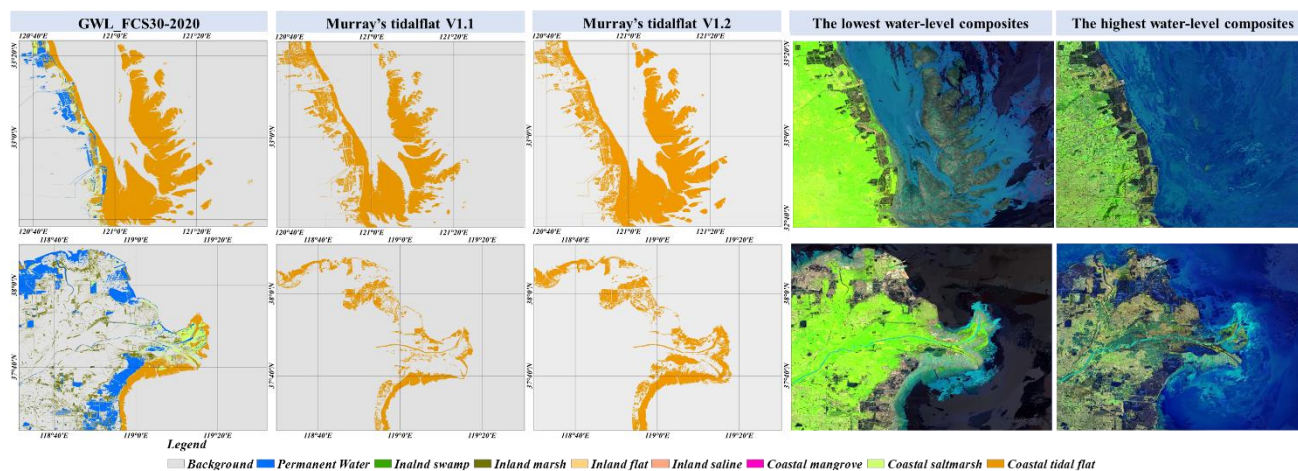


Figure 16. The comparisons between the tidal flat of GWL_FCS30 in 2020, Murray's tidal flat V1.1 in 2016 (Murray et al., 2019), and Murray's tidal flat V1.2 in 2019 (Murray et al., 2022) for two local regions. In each case, the highest and lowest tidal-level composites, composited by SWIR1, NIR, and red bands, are illustrated.

(4) Line 286: These thresholds proposed by Wang et al. 2020 were designed for tidal wetlands, but their application in this study was to inland wetlands. Therefore, the authors need to prove that these thresholds have robust performance in mapping inland wetlands.

Great thanks for the comment. Yes, the rule of 'EVI \geq 0.1, NDVI \geq 0.2, and LSWI $>$ 0' is referenced from the work of Wang et al. (2020) in tidal wetland mapping, actually, whether the rule is also suitable for inland wetlands has been demonstrated on the work of Xiao et al. (2009) and Hao et al. (2022) who used these thresholds to identify the vegetated land-cover types over the inland regions.

Wang, X., Xiao, X., Zou, Z., Hou, L., Qin, Y., Dong, J., Doughty, R. B., Chen, B., Zhang, X., Chen, Y., Ma, J., Zhao, B., and Li, B.: Mapping coastal wetlands of China using time series Landsat images in 2018 and Google Earth Engine, ISPRS J Photogramm Remote Sens, 163, 312-326, <https://doi.org/10.1016/j.isprsjprs.2020.03.014>, 2020.

Xiao, Xiangming, et al. "A simple algorithm for large-scale mapping of evergreen forests in tropical America, Africa and Asia." Remote Sensing 1.3 (2009): 355-374.

Hao, Ying-Ying, et al. "A cascading reaction by hydrological spatial dynamics alternation may be neglected." Environmental Research Letters 17.8 (2022): 084034.

Meanwhile, we also use these thresholds to split the vegetated and non-vegetated areas over several inland regions (including: Poyang Lake, Caspian Sea, Congo Rainforests and so on), Figure S1 illustrates that these thresholds are also robust in splitting vegetated and non-vegetated land-cover types in inland areas. For example, in the First panel over Poyang Lake, the non-vegetated areas (water body, impervious surfaces) are both clearly excluded and these cropland, forest and grassland are completely included. In the second panel over semi-arid region, the bare area and water body are masked while the sparse vegetation (upper left) and inland marsh are included. The third panel in the Congo rainforests, these small rivers and reservoirs are accurately captured.

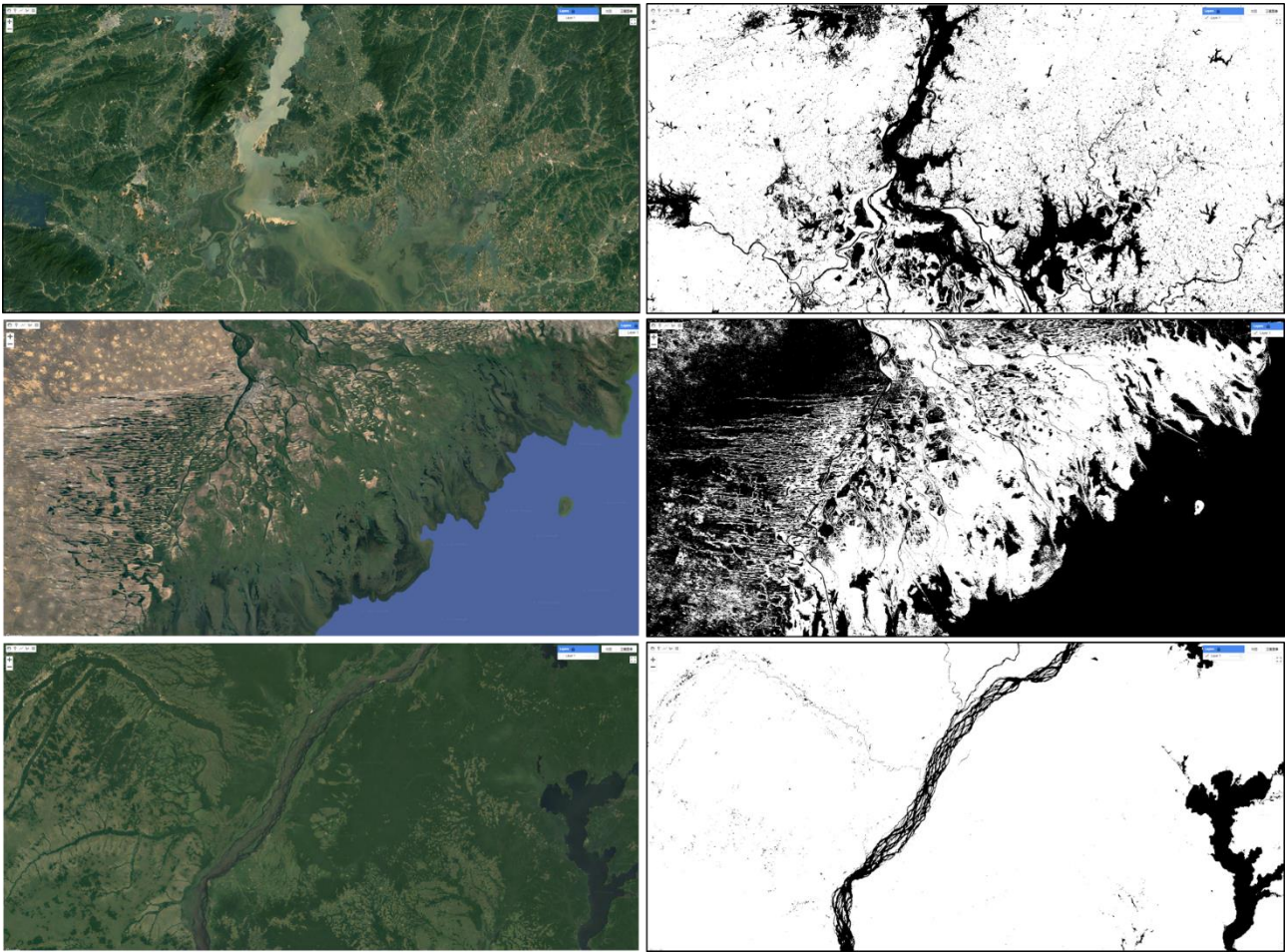


Figure S1. The vegetated and non-vegetated masks (white and black) over three typical inland areas using the rule of ‘ $EVI \geq 0.1$, $NDVI \geq 0.2$, and $LSWI > 0$ ’.

(5) Line 297, Equation 3: This maximum extent of inland wetlands also contains tidal wetlands (since the wetland layer in the global land cover data failed to distinguish them), so how did the authors ensure that the generated samples from inland wetland have corrected labels?

Great thanks for the comment. Yes, the maximum extent of inland wetlands also contains a small amount of tidal wetlands. However, we derive inland training samples from five inland wetland products using a series of refinement measures **instead of directly generating from the inland maximum wetland extents**. Specifically, the consistency analysis of five global wetland datasets (TROP-SUBTROP Wetland, GLWD, CCI_LC, GlobeLand30, and GLC_FCS30) and the temporal stability checking for CCI_LC (1992–2020), GlobeLand30 (2000–2020) and GLC_FCS30 (2015–2020) were applied to identify these temporally stable and high cross-consistency wetland points. It should be noted that the coarse wetland products (GLWD, TROP-SUBTROP and CCI_LC) were resampled to 30 m using the nearest neighbor method on the GEE platform and the coastal wetland layers in these products were excluded. Namely, only the pixel identified as inland wetland in all five products was retained. Then, the morphological erosion filter with a local window of 3×3 was also used to decrease the sampling uncertainty over these land-cover transition areas because the transition zones between two different land-cover types are likely to be misclassified. The details of how to derive inland training samples has been strengthened as:

The pre-existing inland wetland datasets usually suffered from lower accuracy compared to coastal wetland products; for example, the wetland layer in the GlobeLand30-2010 and GLC_FCS30-2015 was validated to achieve a user accuracy of 74.9% (Chen et al., 2015) and 43.4% (Zhang et al., 2021b), respectively. Therefore, **we first generated high-confidence inland wetland samples and then determined their sub-categories (swamp, marsh, inland flat, saline wetland and permanent water). Specifically, the consistency analysis of five global wetland datasets (TROP-SUBTROP Wetland, GLWD, CCI_LC, GlobeLand30, and GLC_FCS30) and the temporal stability checking for CCI_LC (1992–2020), GlobeLand30 (2000-2020) and GLC_FCS30 (2015-2020) were applied to identify these temporally stable and high cross-consistency wetland points ($P_{inlandWet}^{Tstable, Scons}$).** It should be noted that the coarse wetland products (GLWD, TROP-SUBTROP and CCI_LC) were resampled to 30 m using the nearest neighbor method on the GEE platform and the coastal wetland layers in these products were excluded. **Only the pixel identified as inland wetland in all five products was retained. Then, the morphological erosion filter with a local window of 3×3 was also used to decrease the sampling uncertainty over these land-cover transition areas because the transition zones between two different land-cover types are likely to be misclassified (Lu and Wang, 2021; Radoux et al., 2014).**

Afterward, to determine the wetland sub-category for each inland wetland sample, we first used the empirical vegetation rule ($EVI \geq 0.1$, $NDVI \geq 0.2$, and $LSWI > 0$) proposed by Wang et al. (2020) and time-series Landsat imagery to split candidate samples into two parts: vegetated wetland samples (swamp and marsh) and non-vegetated wetland samples (flooded flat, saline and permanent water). Then, as the swamp was defined as the forest or shrubs which grow in the inland freshwater, the global 30-m tree cover dataset (GFCC30TC) was adopted to distinguish the swamp and marsh from vegetated wetland samples. Specifically, if the tree cover of the sample was greater than 30% (Hansen et al., 2013), it was labeled as swamp, and the remaining vegetated wetland samples were labeled as marsh. Furthermore, to distinguish between the inland flat, saline samples and permanent water, the saline blocks in the prior GLWD products were first checked by visual interpretation and then imported as the reference dataset to identify all saline wetland samples. The remaining non-vegetated wetland samples were further refined using the time series of the JRC-GSW datasets, only water probability of these remaining samples less than the threshold of 0.95 (suggested by Wang et al. (2020)) were labeled as flooded flat. Lastly, regarding the permanent water samples, the JRC_GSW water dynamic dataset was validated and achieved producer's and user's accuracies of 99.7% and 99.1% for permanent water (Pekel et al., 2016). The permanent water training samples were directly derived from the JRC_GSW dataset without any refinement rules.

Lastly, although the maximum extent of inland wetlands (Eq. (3)) contains tidal wetlands, our post-processing method also minimize this issue in Section 4.2 as:

As the inland and coastal tidal wetlands were independently produced, some pixels in the overlapping area of maximum inland and coastal wetland extents were simultaneously labeled as inland wetlands and coastal wetlands. However, as the final global wetland map was a hard classification, **these pixels should be post-processed into one label. As the random forest classifier could provide the posterior probability for each pixel, we determined the labels of the confused pixels by comparing the posterior probabilities.**

(6) Section 4.2: The description for obtaining training samples is unclear. What are the strata here, wetland classes or $5^\circ \times 5^\circ$ tiles?

Great thanks for the comment. The description of how to obtain the training samples has been strengthened by your and other reviewer's suggestions. Specifically, we further adjust the Section 3 (Deriving training samples and determining maximum wetland extents) into four parts. In the first three parts, we separately introduce how to derive coastal tidal wetland samples in Section 3.1, inland wetland samples in Section 3.2, and non-wetland samples in Section 3.3, and determine the sample size and distributions. We think the updated manuscript in Section 3 is easier to follow.

As for 'What are the strata here' in Section 4.2, we actually simultaneously consider the wetland classes and $5^{\circ} \times 5^{\circ}$ tiles. To make the local adaptive and stratified modeling more intuitive, the Section 4.2 has been strengthened as:

Since we have simultaneously extracted the maximum coastal and inland wetland extents when deriving training samples from prior wetland datasets, the stratified classification strategy was adopted to fully use the maximum extent constraint. If a pixel was classified as a coastal tidal wetland outside the maximum coastal tidal wetland extents, it would be identified as a misclassification. Furthermore, there were two ideas for the large-area land-cover mapping including global classification modeling (using one universal model for the whole areas) and local adaptive modeling (using various models for different local zones) (Zhang et al., 2020). For example, Zhang and Roy (2017) demonstrated that local adaptive modeling outperformed the global classification modeling strategy. Therefore, the global land surface was first divided into 961 $5^{\circ} \times 5^{\circ}$ geographical tiles illustrated in Figure 5, which were inherited from the global 30 m land-cover mapping by (Zhang et al., 2021b). Then, we trained the local adaptive classification models using derived training samples in Section 3 and multisource and multitemporal features (the highest, lowest water-level and phenological composites and topographical variables) at each $5^{\circ} \times 5^{\circ}$ geographical tile. It should be noted that we used the training samples from neighboring 3×3 geographical tiles to train the classification model and classify the central tile for guaranteeing the spatially continuous transition over adjacent regional wetland maps. Namely, we trained 961 local adaptive classification models and then produced 961 $5^{\circ} \times 5^{\circ}$ wetland maps. Finally, we spatially mosaiced these 961 regional wetland maps into the global 30 m wetland map in 2020.

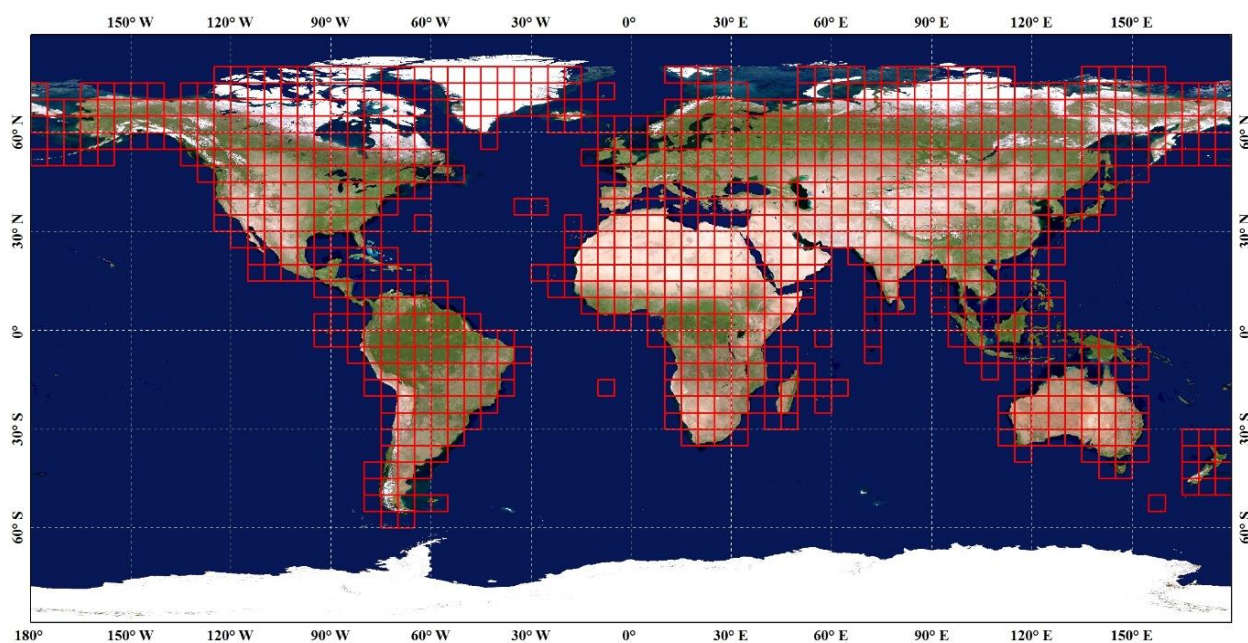


Figure 5. The spatial distribution of 961 $5^\circ \times 5^\circ$ geographical tiles used for local adaptive modeling, which was inherited from the global 30 m land-cover mapping by (Zhang et al., 2021b). The background imagery came from the National Aeronautics and Space Administration (<https://visibleearth.nasa.gov>, last access: 10 Nov 2022).

In addition, the training samples selected from the maximum wetland extent may be of low quality. The authors do explain that the map accuracy is insensitive to low-quality samples within a 20% threshold, but it's still missing a map representing the percentage of real erroneous samples. I think the training samples need to be filtered according to some criterion before classification to improve their accuracy. I recommend clarifying the process of sample generating and the quality-control procedures.

Great thanks for the comment. Yes, we agree that the quality of training samples is important for accurate wetland mapping. In this study, we have used a lot of rules to guarantee the confidence of training samples instead of directly deriving from maximum wetland extents.

Firstly, as for **the mangrove training samples**:

...we first measured the temporal consistency of the three time-series mangrove forest products (CGMFC, GMW, and GBTM mangroves), and only these temporally stable mangrove forest pixels were selected as the primary candidate points ($P_{mangrove}^{Tstable}$). Meanwhile, to minimize the influence of classification error in each mangrove forest product, the cross-consistency of five mangrove products was analyzed, and only the pixel, simultaneously identified as mangrove forest in all five products, was labeled as stable and consistent candidate points ($P_{mangrove}^{Tstable,Scons}$). Furthermore, considering that there was a temporal interval between prior mangrove products and our study, and that mangrove deforestation usually followed the pattern of edge-to-center contraction, a morphological erosion filter with a local window of 3×3 was applied to the $P_{mangrove}^{Tstable,Scons}$ points to further ensure the confidence of mangrove training samples.

Secondly, as for **the tidal flat samples**:

To ensure the accuracy of tidal flat samples, we first applied temporal consistency analysis to the time series of tidal flat datasets from 2000 to 2016 and identified the temporally stable tidal flat pixels ($P_{tidal}^{Tstable}$) during 16 consecutive years. The reason why we discarded the tidal flat datasets before 2000 was that the available Landsat imagery were sparse and could not accurately capture the high-tidal and low-tidal information, and suffered lower monitoring accuracy. Next, [Radoux et al. \(2014\)](#) found that transition zones between two different land-cover types are likely to be misclassified; therefore, the candidate tidal flat samples $P_{tidal}^{Tstable}$ were further refined by the morphological erosion filter with a local window of 3×3 . Furthermore, as a tidal flat is a non-vegetated coastal wetland, we combined the empirical rule ($EVI \geq 0.1$, $NDVI \geq 0.2$, and $LSWI > 0$) proposed by [Wang et al. \(2020\)](#) and time-series Landsat imagery in 2020 (approximately 142 thousand Landsat scenes) to exclude all vegetated pixels from tidal flat training samples.

Thirdly, as for **the salt marsh samples**:

The global distribution of the salt marsh dataset contained 350,985 individual vector polygons and was the most complete dataset on salt marsh occurrence and extent at the global scale (McOwen et al., 2017). However, after careful review, we found some mislabeled salt marsh polygons, so this dataset cannot be used directly to derive training samples. This study first used the random sampling method to generate 35,099 salt marsh points (approximately 10% of the total polygons) based on prior datasets. We combined the visual interpretation method and high-resolution imagery to check each salt marsh point. After discarding the incorrect and uncertain samples, a total of 32,712 salt marsh points were retained.

Fourthly, as for **the inland wetland samples**:

...we first generated high-confidence inland wetland samples and then determined their sub-categories (swamp, marsh, inland flat, saline wetland and permanent water). Specifically, the consistency analysis of five global wetland datasets (TROP-SUBTROP Wetland, GLWD, CCI_LC, GlobeLand30, and GLC_FCS30) and the temporal stability checking for CCI_LC (1992–2020), GlobeLand30 (2000–2020) and GLC_FCS30 (2015–2020) were applied to identify these temporally stable and high cross-consistency wetland points ($P_{inlandWet}^{Tstable, Scons}$). It should be noted that the coarse wetland products (GLWD, TROP-SUBTROP and CCI_LC) were resampled to 30 m using the nearest neighbor method on the GEE platform. Namely, only the pixel identified as inland wetland in all five products was retained. Then, the morphological erosion filter with a local window of 3×3 was also used to decrease the sampling uncertainty over these land-cover transition areas because the transition zones between two different land-cover types are likely to be misclassified (Lu and Wang, 2021; Radoux et al., 2014).

Afterward, to determine the wetland sub-category for each inland wetland sample, we first used the empirical vegetation rule ($EVI \geq 0.1$, $NDVI \geq 0.2$, and $LSWI > 0$) proposed by Wang et al. (2020) and time-series Landsat imagery to split candidate samples into two parts: vegetated wetland samples (swamp and marsh) and non-vegetated wetland samples (flooded flat, saline and permanent water). Then, as the swamp was defined as the forest or shrubs which grow in the inland freshwater, the global 30-m tree cover dataset (GFCC30TC) was adopted to distinguish the swamp and marsh from vegetated wetland samples. Specifically, if the tree cover of the sample was greater than 30% (Hansen et al., 2013), it was labeled as swamp, and the remaining vegetated wetland samples were labeled as marsh. Furthermore, to distinguish between the inland flat, saline samples and permanent water, the saline blocks in the prior GLWD products were first checked by visual interpretation and then imported as the reference dataset to identify all saline wetland samples. The remaining non-vegetated wetland samples were further refined using the time series of the JRC-GSW datasets, only water probability of these remaining samples less than the threshold of 0.95 (suggested by Wang et al. (2020)) were labeled as flooded flat. Lastly, regarding the permanent water samples, the JRC_GSW water dynamic dataset was validated and achieved producer's and user's accuracies of 99.7% and 99.1% for permanent water (Pekel et al., 2016). The permanent water training samples were directly derived from the JRC_GSW dataset without any refinement rules.

Lastly, as for the non-wetland samples:

To automatically derive these non-wetland samples, the multi-epochs GlobeLand30, GLC_FCS30 and CCI_LC global land-cover products were integrated. Specifically, the temporal stability and cross-consistency analysis were applied to three land-cover products to identify temporally stable forest/shrubland, grassland, cropland, and other candidate samples. Furthermore, the morphological erosion filter with the local window of 3×3 was also adopted to decrease the sampling uncertainty over land-cover transition areas.

(7) Section 5.3: The comparison here uses the old-version GMW mangrove map. However, the GMW mangrove map was updated to version 3.0 recently (Bunting et al., 2022), which substantially improved the accuracy by filling gaps caused by the strips in the Landsat-7 images. A detailed comparison with this new version is encouraged.

Great thanks for the suggestion. The new GWM_V3 mangrove map has been used in the revised manuscript as: Figure 14 illustrates the comparisons between our fine wetland maps with three widely used global mangrove forest products (Atlas mangrove, GMW_V3 (Global Mangrove Watch Version3), and USGS Mangrove) listed in Table 1 in two typical mangrove regions (coastal Indonesia and Sundarbans). Intuitively, there was great

consistency over four mangrove datasets because the mangrove forest reflected obvious and strong vegetation reflectance characteristics and was easier to identify than other wetland sub-categories. However, the Atlas mangrove dataset suffers from the underestimation problem; namely, the mangrove area in the Atlas mangrove dataset was obviously lower than the other three products, especially in coastal Indonesia (local enlargements). The USGS mangrove product can comprehensively and accurately capture the spatial distribution of mangroves over two regions. Still, it missed small and isolated fragments of mangrove forests in two regions (green rectangle) based on high-resolution imagery. The GMW_V3 dataset was validated to achieve an overall accuracy of 95.25%, with user and producer accuracies of mangrove forests of 97.5% and 94.0%, respectively (Bunting et al., 2018; Thomas et al., 2017), which shows great agreement with our fine wetland maps and confirms that this dataset accurately identified the spatial patterns of mangrove forest in both regions.

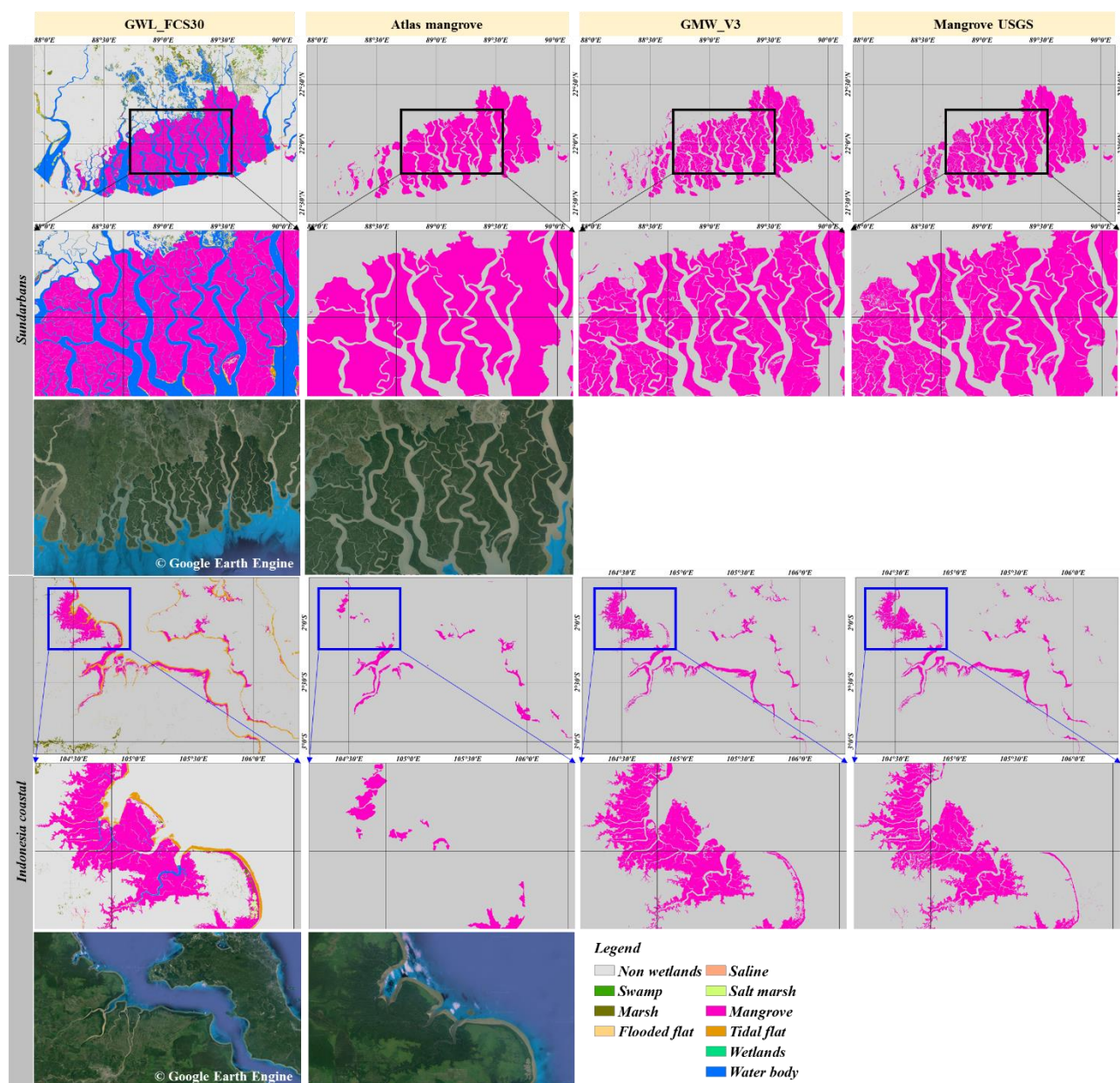


Figure 14. The cross-comparisons between our GWL_FCS30 wetland maps with three mangrove products (Atlas mangrove developed by Spalding (2010), GMW_V3 developed by Bunting et al. (2022) and Mangrove

USGS developed by Giri et al. (2011)) in Sundarbans and coastal Indonesia. The high-resolution imagery came from the Google Earth Engine platform (<https://earthengine.google.com>; last access: 16 May 2022).

Also, a product of global tidal wetland dynamics provided by Murray et al. (2022) could be an important reference for comparison.

Great thanks for the comments. Based on your suggestion, the new global tidal flats in Murray et al. (2022) has been added into the comparisons.

Figure 16 illustrated the comparisons between GWL_FCS30 tidal flat layer with the Murray’s tidal flat V 1.1 in 2016 and the updated Murray’s tidal flat V1.2 in 2019 (Murray et al., 2022) in two local regions, and the corresponding highest and lowest tidal-level composites are also listed. Overall, three products can comprehensively capture the spatial patterns of tidal flats in these two regions, and the GWL_FCS30-2020 and Murray’s tidal flat V1.2 performed higher spatial consistency while the Murray’s tidal flat V1.1 suffered the obvious omission error in three typical areas (red rectangles). Detailedly, we can find that the Murray’s tidal flat products misclassified some coastal ponds and lakes into the tidal flats especially in the first region while the GWL_FCS30-2020 accurately excluded these ponds and lakes.

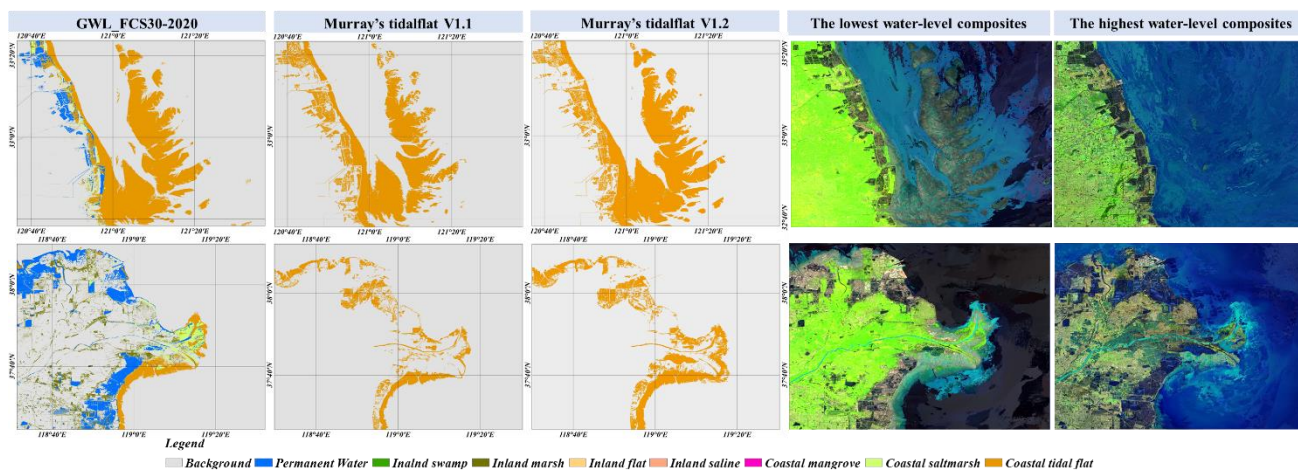


Figure 16. The comparisons between the tidal flat of GWL_FCS30 in 2020, Murray’s tidal flat V1.1 in 2016 (Murray et al., 2019), and Murray’s tidal flat V1.2 in 2019 (Murray et al., 2022) for two local regions. In each case, the highest and lowest tidal-level composites, composited by SWIR1, NIR, and red bands, are illustrated.

(8) Figure 8 lacks a legend.

Great thanks for pointing out the problem. The legend has been added in the Figure 8 as:

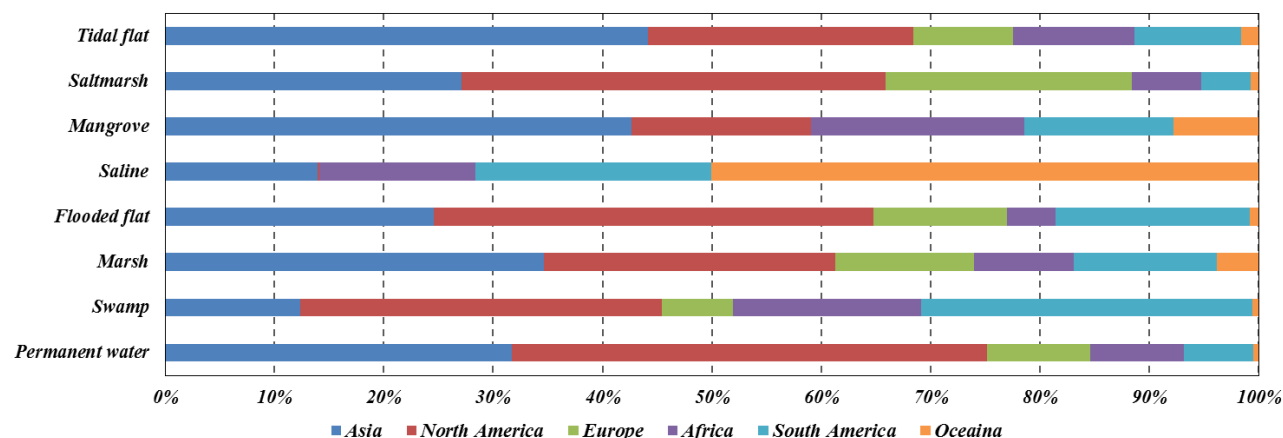


Figure 11. The area proportions of eight wetland sub-categories over each continent.